Measurements and Predictions of Laminar Mixed Convection Flow Adjacent to a Vertical Surface

N. Ramachandran
Assoc. Mem. ASME

B. F. Armaly
Mem. ASME

T. S. Chen
Mem. ASME

Department of Mechanical and Aerospace Engineering,
University of Missouri—Rolla,
Rolla, MO 65401

Measurements and predictions of laminar mixed forced and free convection air flow adjacent to an isothermally heated vertical flat surface are reported. Local Nusselt numbers and the velocity and temperature distributions are presented for both the buoyancy assisting and opposing flow cases over the entire mixed convection regime, from the pure forced convection limit (buoyancy parameter $\xi = Gr_x/Re_x^2 = 0$) to the pure free convection limit ($\xi = \infty$). The measurements are in very good agreement with predictions and deviate from the pure forced and free convection regimes for buoyancy assisting flow in the region of $0.01 \le \xi \le 10$ and for opposing flow in the region of $0.01 < \xi < 0.2$. The local Nusselt number increases for buoyancy assisting flow and decreases for opposing flow with increasing value of the buoyancy parameter. The mixed convection Nusselt numbers are larger than the corresponding pure forced and pure free convection limits for buoyancy assisting flow and are smaller than these limits for opposing flow. For buoyancy assisting flow, the velocity overshoot and wall shear stress increase, whereas the temperature decreases but the temperature gradient at the wall increases as the buoyancy parameter increases. The reverse trend is observed for the opposing flow. Flow reversal near the wall was detected for the buoyancy opposing flow case at a buoyancy parameter of about $\xi = 0.20$.

Introduction

Thermal buoyancy forces play a significant role in forced convection heat transfer when the flow velocity is relatively small and the temperature difference between the surface and the free stream is relatively large. The buoyancy force modifies the flow and the temperature fields and hence the heat transfer rate from the surface.The thermal buoyancy force may be either assisting or opposing the forced flow, depending on the forced flow direction and the surface temperature relative to the free-stream temperature. Mixed convection occurs in many heat transfer devices, such as the cooling system of a nuclear power plant, large heat exchangers, and cooling of electronic equipment. Figure 1 shows a schematic of the two flow cases in which $T_w > T_\infty$ that are considered in this study.

Numerical predictions of mixed convection in laminar boundary layer flow have been reported for vertical, horizontal, and inclined flat plates [1-20]. In these studies, various solution methods, such as a perturbation series, local similarity method, local nonsimilarity method, and finite difference techniques, have been used. On the other hand, few measurements have been reported for this flow geometry [7-10]. Kliegel [7] was the first to report on the measurements of mixed convection flow along an isothermal vertical surface. He employed an interferometric method to measure the local heat transfer, but temperature and velocity distributions were not measured. Gryzagoridis [9] extended the investigation of Kliegel for buoyancy assisting air flow to higher values of the buoyancy parameter, $0 < \xi < 400$, and presented measured local velocity and temperature distributions. He employed hot-wire anemometry to measure the velocity and temperature distributions, but his measured velocities deviated significantly from the numerical predictions [4, 5] at large values of the buoyancy parameter. For example, at a buoyancy parameter of $\xi = 2.0$, the measured velocity deviated by more than 70 percent from the numerical prediction. The significant deviations between measured and predicted velocities at large buoyancy parameters have not been resolved so far.

Measurements of buoyancy opposing mixed convection air flow adjacent to a vertical isothermal surface were reported by Kliegel [7] and more recently by Hishida et al. [10]. Heat transfer data reported by Kliegel deviated significantly from numerical predictions [20] even at small values of the buoyancy parameter. For a buoyancy parameter of $\xi = 0.011$ the measured heat transfer rate deviated by about 35 percent from the numerical prediction. In the latter investigation,

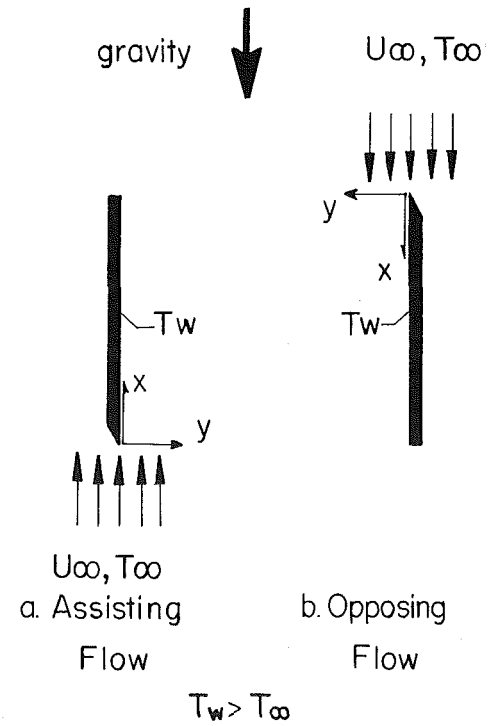

Fig. 1 Schematic of flow geometry

Contributed by the Heat Transfer Division for publication in the JOURNAL OF HEAT TRANSFER. Manuscript received by the Heat Transfer Division March 28, 1984. Paper No. 84-HT-63.

laser-doppler velocimetry was used to measure the velocity distributions, but the temperature distributions in the boundary layer were not measured. The local heat transfer was deduced from measured electric energy input to the surface by correcting for the radiation and conduction losses. Measured results agree favorably with numerical predictions at very small values of the buoyancy parameter, but deviate significantly for larger values of the buoyancy parameter. This deviation could be due to the fact that the heated plate was quite small (16×10 cm) and the air tunnel had a sudden expansion, thus possibly causing the main flow to become turbulent.

The above survey on measurements of laminar mixed convection boundary layer flow adjacent to an isothermal vertical surface clearly demonstrates that simultaneous measurements of velocity and temperature distributions are still needed for both the assisting and the opposing flow cases. This need has motivated the present study.

Experimental Apparatus and Procedure

The experimental investigation was performed in a low-turbulence, open circuit wind tunnel which could be rotated and fixed at any desired inclination angle. The tunnel has a smooth converging nozzle with a contraction ratio of 9:1, a straight test section and a smooth diverging diffuser. Plastic honeycomb material (10.00 cm thick) and several wire screens were used in the front section of the tunnel and along the nozzle length and diffuser to straighten the flow and to reduce the turbulence level in the test section. The free-stream turbulence intensity was measured to be less than 1 percent. The tunnel was constructed from 0.64-cm-thick plexiglass material with adequate frames and supports to provide a rigid structure. Variable speed fans were used at the diffuser end to provide air velocities of 0.3 to 3 m/s through the test section. A schematic of the tunnel is shown in Fig. 2. The test section of the tunnel was instrumented with a hot-wire anemometer system for velocity and temperature measurements. Small channels were machined in the upper side of the test section (instrumented side) to permit passage and movement of the hot-wire probe and its support to any desired location within the test section via a traverse mechanism. During measurements at a selected location, these channels were sealed to provide a smooth upper surface in the test section. The normal motion of the probe (relative to the plane of the heated surface) was controlled by a stepper motor and by a sweep drive unit capable of moving the probe to within 0.02 mm of a desired location. The movement of the probe along the other two directions (along the plate length and across its width) was manually controlled by a lead screw to an accuracy level of 1 mm. This traversing capability was utilized to scan through the boundary layer and throughout the flow domain over the heated surface.

The heated plate consists of four layers which are held together by screws and instrumented to provide an isothermal heated test surface. The upper layer (test surface) is an aluminum plate (30×104 cm and 1.58 cm thick) instrumented with 13 copper-constantan thermocouples. Each thermocouple is inserted into a small hole on the back of the plate and its measuring junction is about 0.3 cm below the testing surface. The middle two layers consist of six heater pads which are backed by a 0.64-cm-thick insulation tiles. The power input to each of the six heating pads is controlled by individual rheostats to maintain a uniform temperature over the entire length of the heated test surface. An aluminum plate, 0.64 cm thick, serves as the bottom layer and as a backing and support to keep the four-layer structure together. The plate assembly is placed in the test section of the wind tunnel and is fastened by screws to the side walls through the backing plate. The rotating tunnel could be placed vertically in either the buoyancy assisting or buoyancy opposing flow condition. Flow visualization, by smoke, indicated the presence of a laminar boundary layer flow adjacent to the vertical plate. The two dimensionality of the flow/thermal field was also verified by measurements. The heated plate could be maintained at a uniform and constant temperature to within 0.1°C by controlling the voltage across the individual heaters. It took approximately 4 hr to reach a steady-state operating condition, and measurements were performed at the center of the test section width.

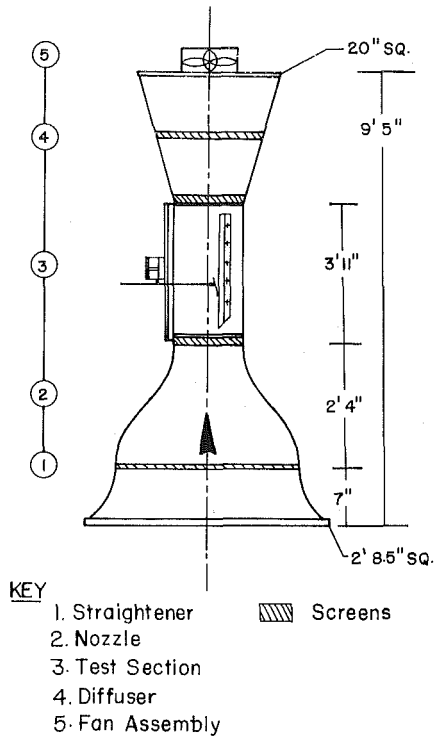

Fig. 2 Schematic of the vertical air tunnel

Nomenclature

C_f = local friction factor
F = reduced stream function, equation (6)
g = gravitational acceleration
Gr_x = $g\beta(T_w - T_\infty)x^3/\nu^2$, local Grashof number
k = thermal conductivity
Nu_x = $q_w x/(T_w - T_\infty)k$, local Nusselt number
Pr = Prandtl number
Re_x = $u_\infty x/\nu$, Reynolds number
T = fluid temperature
T_w = wall temperature
T_∞ = free-stream temperature
u = axial velocity component
u_∞ = free-stream velocity
x = axial coordinate
y = transverse coordinate
α = thermal diffusivity
β = coefficient of thermal expansion
η = pseudo-similarity variable, equation (5)
θ = $(T - T_\infty)/(T_w - T_\infty)$, dimensionless temperature, equation (6)
μ = dynamic viscosity
ν = kinematic viscosity
ξ = $\mathrm{Gr}_x/\mathrm{Re}_x^2$, buoyancy parameter
τ_w = wall shear stress
ψ = stream function, equation (6)

Superscripts

$'$ = denotes partial derivative with respect to η

Velocity and temperature measurements were made by a single DISA boundary-layer probe using the appropriate control bridge (constant resistance and constant current) in the hot-wire anemometer (DISA 55M system). Data acquisition and reduction were performed on a PDP 11/23 computer. The probe was calibrated for the range of velocities and temperatures encountered in the experiment. These calibrations were checked periodically and were repeated if any deviations were detected. The method proposed by Freymuth [21] to interpret hot-wire anemometer output in a thermally stratified flow was used in this study to analyze the output of the hot-wire anemometer during velocity measurements. Additional details regarding this method can be found in [22]. Velocity and temperature profiles were measured for several free-stream velocities and plate temperatures. They were done for both buoyancy assisting and opposing flows and covered wide ranges of the buoyancy parameter.

The uncertainty associated with temperature measurements was determined to be 0.1°C and with velocity measurements was 8 percent for low velocity (0 ~ 0.5 m/sec) and 2 percent for higher velocities.

Numerical Analysis

The problem of laminar mixed convection flow over a heated, isothermal, semi-infinite vertical flat plate has been studied by many investigators [3-11]. The governing conservation equations are given by

$$\frac{\partial u}{\partial x} + \frac{\partial v}{\partial y} = 0 \tag{1}$$

$$u\frac{\partial u}{\partial x} + v\frac{\partial u}{\partial y} = \pm g\beta(T - T_\infty) + \nu\frac{\partial^2 u}{\partial y^2} \tag{2}$$

$$u\frac{\partial T}{\partial x} + v\frac{\partial T}{\partial y} = \alpha\frac{\partial^2 T}{\partial y^2} \tag{3}$$

The boundary conditions for equations (1-3) are

$$u = v = 0;\ T = T_W \text{ at } y = 0$$
$$u \to u_\infty;\ T \to T_\infty \text{ as } y \to \infty \tag{4}$$

The first term on the right-hand side of equation (2) represents the influence of buoyancy, with the plus and minus signs pertaining to thermal buoyancy force assisting and opposing situations, respectively, when $T_w > T_\infty$.

To facilitate the solution of the above set of equations over the regime of mixed forced and free convection, these equations are transformed from the (x, y) coordinates to the $(\xi(x), \eta(x, y))$ coordinates by introducing

$$\xi = \mathrm{Gr}_x/\mathrm{Re}_x^2;\ \eta = y(u_\infty/\nu x)^{1/2} \tag{5}$$

In addition, a reduced stream function $F(\xi,\eta)$ and a dimensionless temperature $\theta(\xi,\eta)$ are defined, respectively, as

$$F(\xi,\eta) = \psi(x,y)/(\nu u_\infty x)^{1/2}$$
$$\theta(\xi,\eta) = (T - T_\infty)/(T_w - T_\infty) \tag{6}$$

where $\psi(x,y)$ is the stream function that satisfies the continuity equation (1). The transformed system of equations is

$$F''' + \frac{1}{2}FF'' \pm \xi\theta = \xi\left(F'\frac{\partial F'}{\partial \xi} - F''\frac{\partial F}{\partial \xi}\right) \tag{7}$$

$$\frac{1}{\mathrm{Pr}}\theta'' + \frac{1}{2}F\theta' = \xi\left(F'\frac{\partial \theta}{\partial \xi} - \theta'\frac{\partial F}{\partial \xi}\right) \tag{8}$$

$$F'(\xi,0) = F(\xi,0) = 0;\ \theta(\xi,0) = 1$$
$$F'(\xi,\infty) = 1;\ \theta(\xi,\infty) = 0 \tag{9}$$

In the foregoing equations, the primes denote partial differentiation with respect to η.

The primary physical quantities of interest are the local

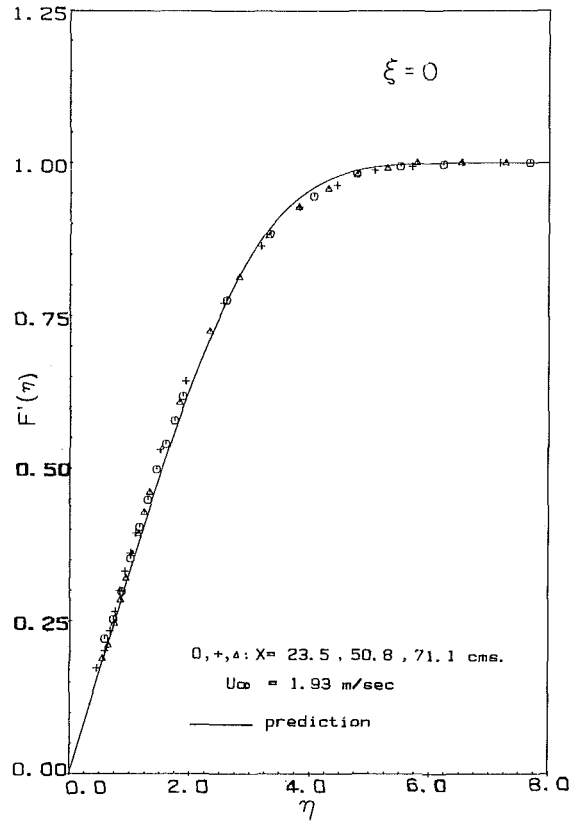

Fig. 3 Velocity distribution, forced convection limit

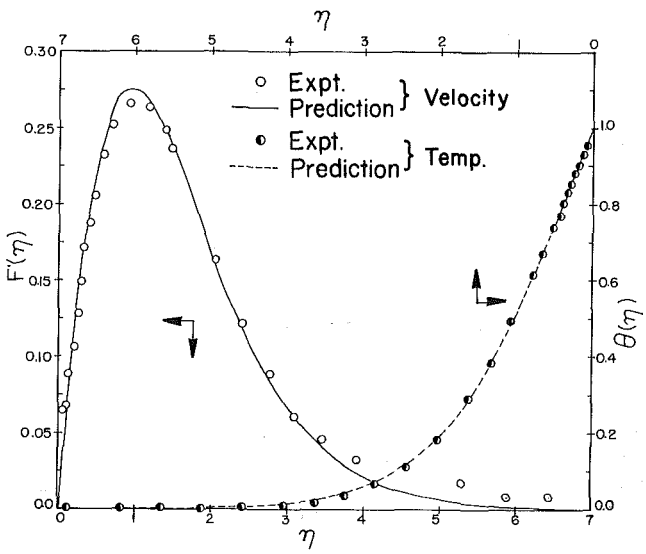

Fig. 4 Velocity and temperature distributions, free convection limit

Nusselt number Nu_x, the local friction factor C_f, the velocity distribution $u/u_\infty = F'(\xi,\eta)$, and the temperature distribution $\theta(\xi,\eta)$. The first two quantities can be expressed, respectively, by

$$\mathrm{Nu}_x\mathrm{Re}_x^{-1/2} = -\theta'(\xi,0);\ C_f\mathrm{Re}_x^{1/2} = 2F''(\xi,0) \tag{10}$$

Local similarity and local nonsimilarity solution techniques have been employed in earlier investigations [4, 23] of the same problem. In the present investigation the governing equations were solved by a finite difference solution scheme which is a modified version of that developed by Keller and Cebeci [24, 25]. The use of this solution scheme, which has been successfully employed in [19], provided a more accurate solution for a wider range of buoyancy parameters.

For low buoyancy parameters the three solution methods

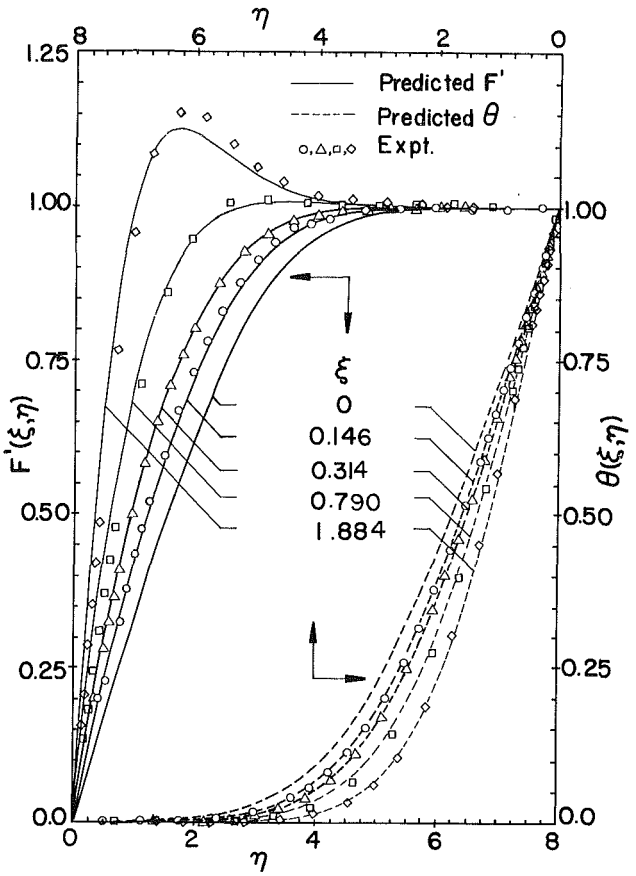

Fig. 5 Velocity and temperature distributions for buoyancy assisting case

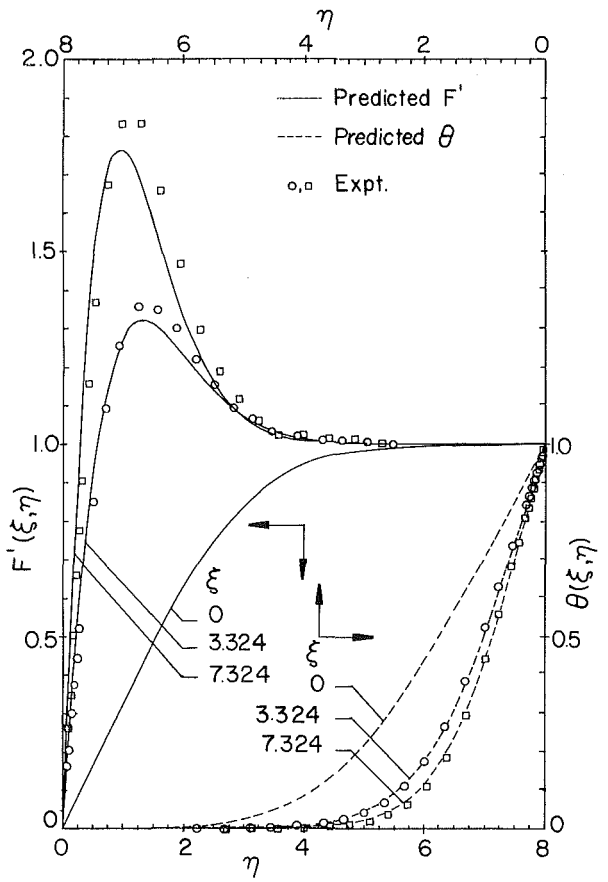

Fig. 6 Velocity and temperature distributions for buoyancy assisting case

provide identical results, but as the buoyancy parameter increases deviations occur. For example, at a buoyancy parameter of unity, $\xi = 1$, $F''(\xi,0)$ deviates from the local similarity value by 12.6 percent when using a local non-similarity method and by 15.7 percent when using a finite difference method. Under the same conditions, $\theta'(\xi,0)$ deviates only by 2.2 percent and by 1.7 percent, respectively. Numerical solutions were carried out for the same values of the buoyancy parameter ξ as those obtained during the experiment, thus eliminating the need of any interpolations. The Prandtl number used in the computations was 0.70.

Results and Discussion

To test the operation of the wind tunnel and its instrumentation, the pure forced and the pure free convection cases were measured. The measured and the predicted values are compared for pure forced convection, $\xi = 0$, in Fig. 3. Similarly, the measured and predicted [26] values for the pure free convection case, $\xi = \infty$, are compared in Fig. 4. It is evident from these two figures that the measurements are in very good agreement with predictions, thus validating the performance of the wind tunnel and its instrumentation.

The velocity and temperature distributions for the buoyancy assisting case were measured for buoyancy parameter ξ in the range of $0 < \xi < 16$. The highest value of the buoyancy parameter was limited by the maximum, safely attainable plate temperature of 95°C and the lowest velocity of 0.3 m/s. For this case of buoyancy assisting flow, the air tunnel was placed in the vertical direction, with air suction from the top and the leading edge of the plate facing down. Representative velocity and temperature profiles for the assisting flow case are shown in Figs. 5-7. In all these figures, the solid and the dashed lines represent, respectively, the predicted velocity and temperature distributions from the numerical solution of equations (7-9) for the indicated value

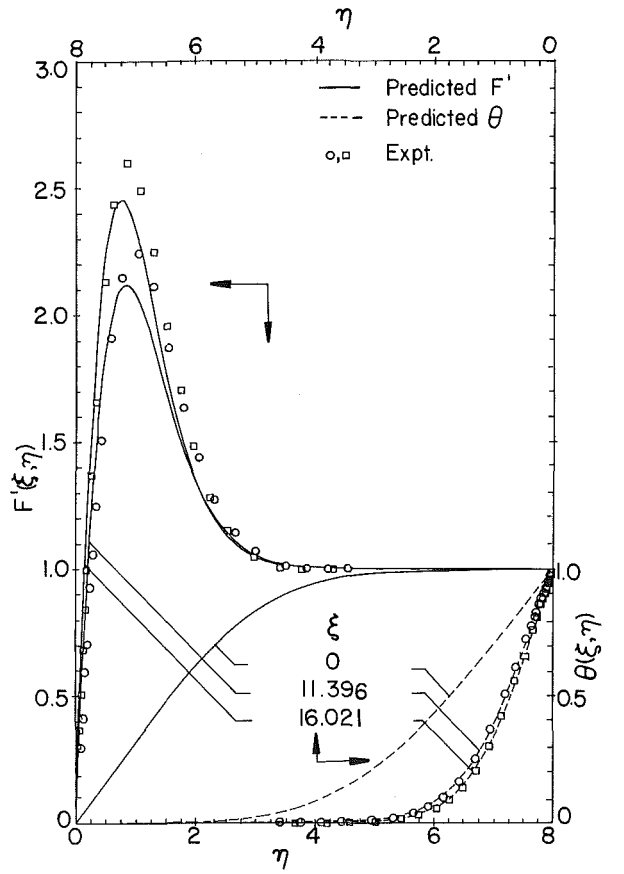

Fig. 7 Velocity and temperature distributions for buoyancy assisting case

of the buoyancy parameter. The predicted velocity and temperature distributions for pure forced convection ($\xi = 0$) are presented in each figure for comparison. Measured velocity and temperature data were reduced and transformed into the ξ, η coordinate system for comparison with the predicted values. Fluid properties were evaluated at the film temperature $T_f = (T_W + T_\infty)/2$. These figures demonstrate that measured velocity and temperature distributions are in very good agreement with the predictions. The agreement between the measured and the predicted temperature distributions is better than that for the velocity distributions. The velocity field is seen to be more sensitive to changes in the value of the buoyancy parameter than the temperature field and this sensitivity increases as the buoyancy parameter increases. It can be seen from these figures that as the buoyancy parameter increases, both the velocity and temperature boundary layer thicknesses decrease and the velocity and temperature gradients at the wall increase, causing an increase in both the local wall shear stress and the local surface heat transfer rate. It is also evident that the measured velocity distributions show a slightly higher overshoot than the predictions. For example, at a buoyancy parameter of $\xi = 16.021$ the experimental results deviate by 6.12 percent from the predicted values.

The vertical air tunnel which was used to study the buoyancy assisting mixed convection flow was rotated 180 deg in order to examine the buoyancy opposing flow case. For this case the suction fan was at the bottom of the tunnel and the leading edge of the plate was pointing upward toward the inlet section of the tunnel. Measurements in this case were limited to a buoyancy parameter range of $0 \leq \xi \leq 0.2$, because flow reversal occurs when $\xi > 0.2$. The hot-wire anemometer is not sensitive to the flow direction and thus could not be used to measure the flow reversal in such a region. In fact, the governing equations for this case also failed to yield converged numerical solutions for values of buoyancy parameter larger than $\xi = 0.18$, because the model cannot be used in regions where flow reversal occurs. Flow visualization by smoke injections confirmed the existence of a reversed flow region at a buoyancy parameter of 0.20. Measured velocity and temperature distributions for the opposing flow case are presented in Fig. 8. In that figure the solid and the dashed lines represent, respectively, the velocity and temperature distribution predicted by the numerical solution of equations (7-9) for the indicated value of the buoyancy parameter. Measured velocities and temperatures are seen to be in reasonable agreement with the predicted values (within 10 percent), but this agreement is not as good as the one reported for the buoyancy assisting flow case. As the buoyancy parameter increases, the velocity and temperature gradients at the wall decrease, causing a decrease in both the local wall shear stress and the local surface heat transfer rate. The measured results for a buoyancy parameter of 0.208 are presented in Fig. 8 and they clearly demonstrate the existence of a separated region near the wall. Predicted results are not presented for this value because a converged solution could not be obtained beyond a value of $\xi = 0.18$. The data reported by Kliegel [7] indicate flow separation at about $\xi = 0.2$ which agrees with the present findings. Hishida et al. [10] observed a similar behavior in their experimental study of this geometry, but they concluded that a laminar boundary layer existed up to a buoyancy parameter value of $\xi = 0.25$, which seems to be higher than the present findings. At this time it is not clear to the authors how Hishida et al. [10] were able to predict the reversed flow via the normal parabolic governing equations.

The measured temperature distribution was used to determine the temperature gradient at the wall which was in turn utilized to determine the local Nusselt number. The uncertainty associated with determining the temperature gradient at the wall and consequently the Nusselt number was

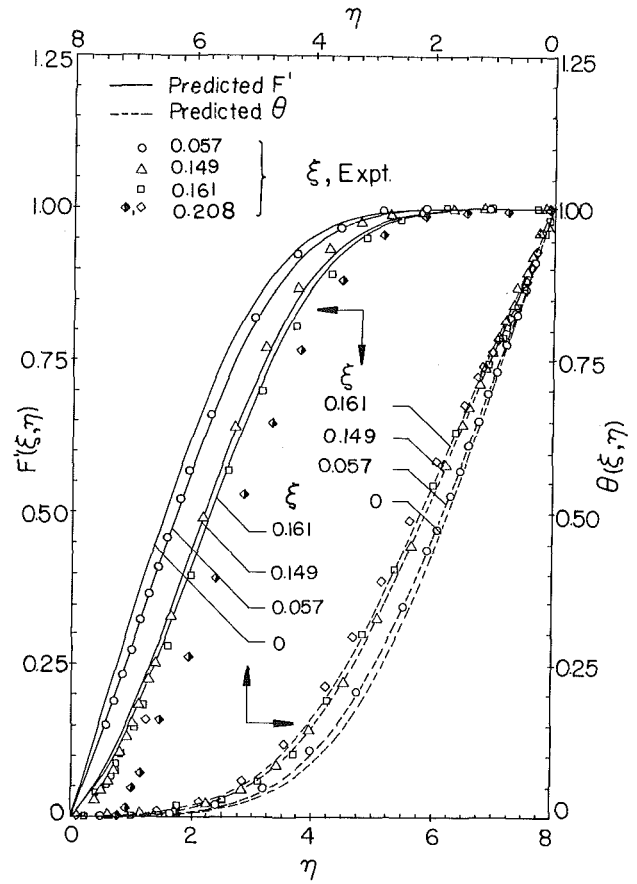

Fig. 8 Velocity and temperature distributions for buoyancy opposing case

determined to be less than 5 percent. The variation of the deduced Nusselt number as a function of the buoyancy parameter is presented in Fig. 9. A sample of data reported by Kliegel [7] is also presented for comparison. As can be seen from the figure, the agreement between the experimental and the predicted local Nusselt numbers is very good for both the present study and that of Kliegel [7]. For buoyancy assisting flow, the mixed forced and free convection results asymptotically approach the pure forced ($\xi = 0$) and the pure free ($\xi = \infty$) convection limits, and the mixed convection Nusselt numbers are higher than the equivalent pure forced or pure free convection flow. An increase in the buoyancy parameter results in a higher velocity overshoot, a steeper temperature gradient at the wall and hence a higher Nusselt number. As pointed out in [4, 9], the regime of mixed convection is represented by the buoyancy parameter range of $0.10 \leq \xi \leq 3.0$ when based on a 5 percent departure from pure forced and pure free convection results. However, the actual deviations from the pure convection results occur in the region of $0.01 \leq \xi \leq 10$, as can be seen from Fig. 9. The local Nusselt numbers can be 25 percent higher than the corresponding pure forced or pure free convection values in this region of buoyancy assisting flow. The local Nusselt number variation with the buoyancy parameter for the buoyancy opposing flow case is also shown in Fig. 9, along with the numerically predicted values. Good agreement (better than 10 percent) is seen between the experimental and the predicted values. The reported results by Kliegel [7] for these conditions deviate significantly, 35 percent, from the predicted values. As the buoyancy parameter increases, the heat transfer decreases gradually and then rapidly in the vicinity of $\xi = 0.20$, when flow reversal starts to occur. In that region the mixed convection Nusselt number deviates by more than 40 percent from the pure forced convection value. For the buoyancy opposing flow case, the mixed convection Nusselt numbers

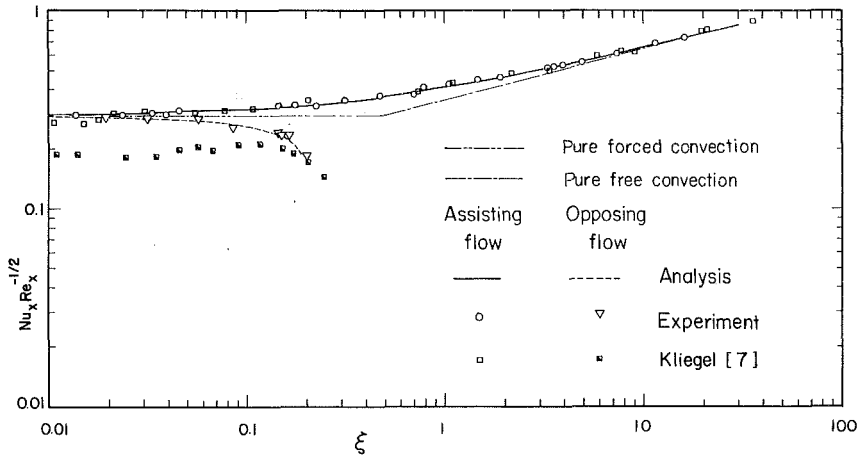

Fig. 9 Measured and predicted mixed convection regime

are lower than the corresponding pure forced convective values.

Conclusions

In the present study, representative velocity and temperature distributions were measured and local Nusselt numbers obtained for laminar mixed convection flow of air adjacent to a heated, isothermal vertical plate for both the buoyancy assisting and the buoyancy opposing flow cases. Measurements were also conducted for pure forced convection and pure free convection from this geometry, and these measurements represent the two limiting cases of the mixed convection regime. A comparison between the measured and the predicted temperature and velocity profiles reveals a very good agreement between the two, with a maximum velocity deviation of less than 6.2 percent. The local Nusselt number has been found to increase with increasing buoyancy parameter for the buoyancy assisting flow and to decrease for the buoyancy opposing flow. The mixed convection Nusselt numbers are always higher for buoyancy assisting flow (with deviations of 25 percent) and are lower for buoyancy opposing flow (with deviations of 40 percent) than the corresponding values for pure forced or pure free convection. The velocity distributions for the buoyancy assisting flow exhibit a significant overshoot above the free-stream value. In addition, the velocity field has been found to be more sensitive to the buoyancy effect than the temperature field. The mixed convection domain, defined as the region where the Nusselt numbers resulting from mixed convection calculations deviate by more than 5 percent from either the pure forced or the pure free convection values, is given by $0.1 \leq \xi \leq 3.0$ for the assisting flow case. A very good agreement between the measured and the predicted results has been obtained for both the assisting and opposing flow cases.

Acknowledgments

This study was supported in part by grants from the National Science Foundation (NSF MEA 83-00785 and NSF MEA 81-11673).

References

1 Sparrow, E. M., and Gregg, J. L., "Buoyancy Effects in Forced-Convection Flow and Heat Transfer," ASME *Journal of Applied Mechanics*, Vol. 81, 1959, pp. 133-134.

2 Szewczyk, A. A., "Combined Forced and Free Convection Laminar Flow," ASME JOURNAL OF HEAT TRANSFER, Vol. 86, 1964, pp. 501-507.

3 Merkin, J. H., "The Effect of Buoyancy Forces on the Boundary-Layer Flow Over a Semi-Infinite Vertical Flat Plate in a Uniform Free Stream," *Journal of Fluid Mechanics*, Vol. 35, 1969, pp. 439-450.

4 Lloyd, J. R., and Sparrow, E. M., "Combined Forced and Free Convection Flow on Vertical Surfaces," *International Journal of Heat and Mass Transfer*, Vol. 13, 1970, pp. 434-438.

5 Oosthuizen, P. H., and Hart, R., "A Numerical Study of Laminar Combined Convective Flow Over Flat Plates," ASME JOURNAL OF HEAT TRANSFER, Vol. 95, 1973, pp. 60-63.

6 Wilks, G., "Combined Forced and Free Convection Flow on Vertical Surfaces," *International Journal of Heat and Mass Transfer*, Vol. 16, 1973, pp. 1958-1964.

7 Kliegel, J. R., "Laminar Free and Forced Convection Heat Transfer from a Vertical Flat Plate," Ph.D. Thesis, University of California, Berkeley, 1959.

9 Babezha, A. V., Gimbutis, G. I., and Shvenchyanas, P. P., "Heat Transfer at a Vertical Flat Surface with the Combined Effect of Forced and Free Convection in the Same Direction," *Institute of Chemical Engineering*, Vol. 21, No. 1, 1981, pp. 135-138.

9 Gryzagoridis, J., "Combined Free and Forced Convection from an Isothermal Vertical Plate," *International Journal of Heat and Mass Transfer*, Vol. 18, 1975, pp. 911-916.

10 Hishida, K., Yoshida, A., and Maeda, M., "Buoyancy Effects on Boundary Layer Flow and Forced Convective Heat Transfer Over a Vertical Isothermally Heated Plate," Presented at the ASME-JSME Thermal Engineering Joint Conference, Honolulu, Hawaii, March 20-24, 1983, Vol. 3, pp. 163-168.

11 Sparrow, E. M., and Minkowycz, W. J., "Buoyancy Effects on Horizontal Boundary-Layer Flow and Heat Transfer," *International Journal of Heat and Mass Transfer*, Vol. 5, 1962, pp. 505-511.

12 Mori, Y., "Buoyancy Effects in Forced Laminar Convection Flow Over a Horizontal Flat Plate," ASME JOURNAL OF HEAT TRANSFER, Vol. 83, 1961, pp. 479-482.

13 Hauptmann, E. G., "Laminar Boundary-Layer Flows With Small Buoyancy Effects," *International Journal of Heat and Mass Transfer*, Vol. 8, 1965, pp. 289-295.

14 Redekopp, L. G., and Charwat, A. F., "Role of Buoyancy and the Boussinesq Approximation in Horizontal Boundary Layers," *Journal of Hydronautics*, Vol. 6, 1972, pp. 34-39.

15 Leal, L. G., "Combined Forced and Free Convection Heat Transfer from a Horizontal Flat Plate," *Journal of Applied Mechanics and Physics (ZAMP)*, Vol. 24, 1973, pp. 20-42.

16 Hieber, C. A., " Mixed Convection Above a Heated Horizontal Surface," *International Journal of Heat and Mass Transfer*, Vol. 16, 1973, pp. 769-785.

17 Robertson, G. E., Seinfeld, J. H., and Leal, G. E., "Combined Forced and Free Convection Flow Past a Horizontal Flat Plate," *AIChE Journal*, Vol. 19, 1973, pp. 998-1008.

18 Chen, T. S., Sparrow, E. M., and Mucoglu, A., "Mixed Convection in Boundary Layer Flows on a Horizontal Plate," ASME JOURNAL OF HEAT TRANSFER, Vol. 99, 1977, pp. 66-71.

19 Mucoglu, A., and Chen, T. S., " Mixed Convection on Inclined Surfaces," ASME JOURNAL OF HEAT TRANSFER, Vol. 101, 1979, pp. 422-426.

20 Moutsoglou, A., Tzuoo, S. K. L., and Chen, T. S., "Mixed Convection in Boundary Layer Flows Over Inclined Surfaces," *AIAA 15th Thermophysics Conference*, Snowmass, Colorado, July 14-16, 1980, Paper No. AIAA-80-1525.

21 Freymuth, P., "Hot-Wire Anemometer Thermal Calibration Errors," *Instruments and Control Systems*, Oct. 1970, pp. 82-83.

22 Ramachandran, N., "Measurements and Predictions of Laminar Mixed Convection from Flat Surfaces," M. S. Thesis, University of Missouri, Rolla, 1983.

23 Chen, T. S., and Mucoglu, A., "Buoyancy Effects on Forced Convection Along a Vertical Cylinder," ASME JOURNAL OF HEAT TRANSFER, Vol. 97, 1975, pp. 198-203.

24 Keller, H. B., and Cebeci, T., "Accurate Numerical Methods for Boundary Layer Flows. I: Two-Dimensional Laminar Flows," *Proceedings of 2nd International Conference on Numerical Methods in Fluid Dynamics*, Springer-Verlag, Berlin, 1971.

25 Keller, H. B., and Cebeci, T., "Accurate Numerical Methods for Boundary Layer Flows. II: Two-Dimensional Turbulent Flows," *AIAA Journal*, Vol. 10, 1972, pp. 1193-1199.

26 Ostrach, S., "An Analysis of Laminar Natural Convection Flow and Heat Transfer About a Flat Plate Parallel to the Direction of the Generating Body Forces," NACA TN 2635, 1952.